Inhibition of Renin-Angiotensin System (RAS) Reduces Ventricular Tachycardia Risk by Altering Connexin43

Short title: Iravanian. RAS and arrhythmias

Shahriar Iravanian[1], Ali A Sovari[2], Harvey A Lardin[2], Hong Liu[2], Hong D. Xiao[3], Elena Dolmatova[4], Zhe Jiao[1], Brett S. Harris[5], Emily A. Witham[6], Robert G. Gourdie[5], Heather S. Duffy[4], Kenneth E. Bernstein[7], Samuel C. Dudley Jr.[2†]

[1] Division of Cardiology, Atlanta Veterans Affairs Medical Center, and Emory University, Atlanta, GA, 30033

[2] Division of Cardiology, University of Illinois at Chicago, Chicago, IL, 60612

[3] Department of Pathology, Massachusetts General Hospital, Boston, MA 02114

[4] Division of Cardiology, Beth Israel Deaconess Medical Center, Boston MA 02115

[5] Department of Cell Biology and Anatomy, Medical University of South Carolina, Charleston, SC, 29425

[6] Biomedical Sciences Graduate Program, University of California San Diego, La Jolla, California 92093

[7] Cedars-Sinai Medical Center - Departments of Pathology and Biomedical Sciences, Los Angeles, CA 90048

[†]**Correspondence to:**
Samuel C. Dudley, Jr., M.D., PhD
Professor and Chief
Section of Cardiology, University of Illinois at Chicago
840 S. Wood Street
M/C 715
Chicago, IL 60612
Tel: (312) 413-8870
Fax (312) 413-2948
Email: scdudley@uic.edu

Abstract

Aims: Renin-angiotensin system (RAS) activation is associated with arrhythmias. We investigated the effects of RAS inhibition in cardiac-specific angiotensin converting enzyme (ACE) overexpression (*ACE 8/8*) mice, which exhibit proclivity to ventricular tachycardia (VT) and sudden death because of reduced connexin43 (Cx43).

Methods and Results: ACE 8/8 mice were treated with an ACE inhibitor (captopril) or an angiotensin receptor type-1 blocker (losartan). Subsequently, electrophysiological studies were performed, and the hearts were extracted for Cx43 quantification using immunoblotting, immunohistochemistry, fluorescent dye spread method and sodium current quantification using whole cell patch clamping. VT was induced in 12.5% of captopril treated *ACE 8/8* and in 28.6% of losartan treated mice, compared to 87.5% of untreated mice ($P<0.01$). Losartan and captopril treatment increased total Cx43 2.4-fold ($P=0.01$) and the Cx43 phosphorylation ratio 2.3-fold ($P=0.005$). Treatment was associated with a recovery of gap junctional conductance. Survival in treated mice improved to 0.78 at 10 weeks (95% confidence interval 0.64 to 0.92), compared to the expected survival of less than 0.50.

Conclusions: In a model of RAS activation, arrhythmic risk was correlated with reduced Cx43 amount and phosphorylation. RAS inhibition resulted in increased total and phosphorylated Cx43, decreased VT inducibility, and improved survival.

Introduction

In humans, ventricular tachyarrhythmias, especially in the setting of low left ventricular ejection fraction, are linked to renin-angiotensin system (RAS) activation [1]. Conversely, inhibiting RAS has a protective effect against arrhythmia. Treatment of high-risk patients with the angiotensin converting enzyme (ACE) inhibitor (ACEI), ramipril, is associated with a relative risk reduction of 0.66 in the incidence of sudden cardiac death [2]. Similarly, other RAS modifiers, such as mineralocorticoid receptor blockers, have shown promise in reducing the burden of ventricular arrhythmias [3,4].

The mechanisms underlying the proarrhythmic effects of RAS activation are not known, however. Traditionally, the effect of RAS on promoting atrial and ventricular arrhythmias is explained based on increased cardiac hypertrophy, fibrosis, and heterogeneity of the cardiac tissue [5]. Nevertheless, such models fail to explain the observed reversal of the proarrhythmic effects upon treatment with ACEIs or angiotensin II (AngII) receptor blockers (ARBs), suggesting other electrophysiological effects of RAS activation. Proposed mechanisms include direct or indirect effects of AngII and aldosterone on membrane ion channels [6,7], suppression of the sarcoplasmic reticulum Ca^{2+}-ATPase (SERCA) pump [8] or the ryanodine receptor (Ryr2) [9,10], and disruption of cell-to-cell coupling through modification of gap junctional conductance.

Previously, we have described the effects of a model of RAS activation in the heart brought about by cardiac-specific overexpression of ACE. These mice (*ACE 8/8* mice) have increased ACE in the atria and ventricles, accompanied by a four-fold increase in

the level of AngII in the heart. They suffer from low voltage atrial activity, advanced atrioventricular (AV) block, an increased tendency to ventricular tachycardia (VT) during programmed stimulation, and an increased risk of sudden death due to spontaneous VT or ventricular fibrillation (VF) [11]. The major biochemical abnormality in these mice is a severe reduction and abnormal phosphorylation of ventricular connexin 43 (Cx43) [12]. Nevertheless, it is not clear that this abnormality is responsible for the increased arrhythmic risk in this model of RAS activation.

Cx43 is a major component of the ventricular gap junctional complexes. Like other connexins, it forms hexameric hemichannels. After translocation to the membrane, two hemichannels from adjacent cardiac cells meet head-to-head across the extracellular space and provide a low resistance pathway for electrical conduction between myocytes [13]. Along with sodium current, coupling by Cx43 determines the conduction velocity in the ventricles [14].

Reduction or abnormal distribution of Cx43 has been observed in various pathological conditions, including cardiomyopathies [15], ventricular hypertrophy [16] and in infarct border zone [17]. Reduced expression of Cx43 can slow conduction velocity, increase heterogeneity, and exaggerate anisotropic properties of ventricles, promoting tachyarrhythmias [18]. The latter two effects facilitate wave break and reentry initiation, whereas the reduction in conduction velocity shortens the reentry wavelength and promotes its maintenance [19].

Cx43 is usually phosphorylated on multiple serine/threonine and tyrosine sites [20,21]. Phosphorylation of Cx43 is necessary for its proper assembly into connexon hexamers and for transport and insertion into the membrane. In addition, phosphorylation and dephosphorylation have a significant effect on gap junctional conductance, selectivity, and recycling [22,23]. Abnormal phosphorylation status, either dephosphorylation or phosphorylation at certain sites such as Ser368, is associated with reduced Cx43 function [20] and increased arrhythmic risk.

In this paper, we test the hypothesis that pharmacological inhibition of RAS reverses the proclivity to ventricular tachyarrhythmias in *ACE 8/8* mice by correcting abnormalities of the quantity and function of Cx43.

Materials and Methods

Transgenic mice model

The details of the generation of *ACE 8/8* mice have been published already [11]. These mice were made by targeted homologous recombination in embryonic stem (ES) cells. In summary, a fragment of genomic mouse DNA, containing the somatic ACE promoter, somatic ACE transcription start site, and exons 1-12 of the ACE gene was cloned. A neomycin cassette was inserted in a BssH II restriction site within the ACE promoter and acts to block transcription from the natural somatic ACE promoter. The α-myosin heavy chain (α-MHC) promoter was cloned downstream of the neo cassette and controls somatic ACE expression. The targeting construct was electroporated into 129/SVx129/SvJ ES cells. The chimeric mice were mated to C57/BL6 mice. All studies were performed on F2 or later generation wild-type (*WT*) and homozygote (*ACE 8/8*) mice. Heterozygote (*ACE 8/WT*) mice exhibit a mild non-fatal phenotype and are not included in the current study.

Substitution of the somatic ACE promoter with the α-MHC promoter has been reported to localize the expression of ACE to heart and results in a 4-fold increase in cardiac AngII in homozygote mice. This level is comparable to the range seen in human pathological states [24]. Beside the marked electrophysiological abnormalities, the phenotype in the homozygote mice includes decreased systolic blood pressure, enlarged atria, normal ventricular size and function, and a lack of ventricular fibrosis or abnormal structure in histological sections of the heart.

Pharmacological interventions

Animal procedures were approved by the Emory University, University of Illinois at Chicago, or the Atlanta Veterans Administration Medical Center Institutional Animal Care and Use Committees. Four-week old mice (*ACE 8/8* or *WT* littermates) of either sex were divided into three groups. The first group received the ACEI, captopril (Sigma, St. Louis, MO), at a dose of 400 mg/L in the drinking water. The second group was treated with an ARB, losartan (Axxora, San Diego, CA), at a dose of 500 mg/L in the drinking water. Captopril and losartan were given from weeks four to ten. The third group remained untreated.

All three groups were followed until week 10, when they underwent electrocardiography (ECG) and invasive electrophysiology studies (EPS). Afterward, the mice were sacrificed, and the hearts were extracted for further analysis.

Electrophysiological study

Ten-week old mice underwent a detailed EPS. Mice were anesthetized using an intraperitoneal injection of ketamine (100 mg/kg) and xylazine (5 mg/kg). After cutdown, a 1.1 F octapolar catheter with 0.5 mm inter-electrode spacing (EPR 800, Millar Instruments, Houston, TX) was placed into the right jugular vein and was advanced into the right ventricle. Six limb-lead ECG and intracardiac electrograms were recorded using a Prucka CardioLab 4.1 system with a sampling rate of 1000 Hz and digitalized at 12 bits resolution. A constant current stimulator (A320, World Precision Instruments, Sarasota, FL) connected to a laptop computer was used for cardiac stimulation. During the

experiment, body temperature was maintained at 37ºC using a warming pad. Recording with less stringent low pass filtering than used in this study (i.e. 400 Hz for intracardiac and 100 Hz for surface ECG) confirmed that the differences among groups were unaffected by aliasing.

Baseline six-lead ECG and EPS allowed for measurements of sinus cycle length, QRS duration, QT interval, frontal axis, and frontal plane QRS vector amplitude. QRS amplitude, defined as the amplitude of the first major deflection of the QRS complex, was measured using a signal averaging technique to improve signal-to-noise ratios. An automatic algorithm (using maximum first derivative technique) detected the fiducial point for each QRS complex. An artifact-free segment of ECG, containing 50-100 beats, was selected, and all the QRS complexes in this segment were averaged. Leads I and aVF were combined according to $\sqrt{I^2 + aVF^2}$ to derive the frontal plane QRS vector amplitude. Previously, we established that the QRS amplitude in *ACE 8/8* mice is inversely related to the severity of the phenotype and risk of VT and sudden death [12].

A S1-S2 protocol (eight S1 beats at a cycle length of 100 ms followed with one S2 at different coupling intervals) at twice the capture threshold was performed to measure ventricular refractory period (VERP). Two different programmed ventricular stimulation protocols were employed to test for VT inducibility: burst pacing at cycle lengths 75 ms down to 45 ms for twelve beats or eight beats at 50 ms followed by four beats at 30 ms (Fig. 1) [25]. During the pilot phase of the study, it was determined that using a drive

train with double or triple extrastimuli did not provide additional information regarding VT inducibility in this model.

The catheter was finely manipulated to detect the His potential. AH and HV intervals were measured from the intracardiac electrograms.

Western blotting

After EPS was performed, mice were euthanized, and hearts were extracted. The ventricular tissue was homogenized in a buffer containing 20 mM Tris-Cl pH 7.4, 150 mM NaCl, 2.5 mM EDTA, 1% Triton-100, 10 μL/ml PMSF, 10 μL/ml protein inhibitor cocktail (Pierce, Rockford, IL) and 10 μL/ml phosphatase inhibitor cocktail II (Sigma). Protein samples (5-20 μg) were separated on 10% SDS-PAGE gels and transferred to nitrocellulose membranes. The membranes were blotted with anti-Cx43 (Sigma) at dilution of 1:10000-1:20000. For a loading control, anti-glyceraldehyde-3-phosphate dehydrogenase (GAPDH) at a dilution of 1:2000-1:5000 (Santa Cruz Biotech, Santa Cruz, CA) was used. After treatment with HRP-conjugated secondary anti-rabbit or anti-mouse antibodies at 1:2000, the membranes were exposed to X-ray film using the enhanced chemiluminescence (ECL) method. The X-ray film images were scanned and analyzed with NIH ImageJ software.

Cx43 has multiple phosphorylated forms with different electrophoretic speeds. The non-phosphorylated form and Cx43 phosphorylated at Ser368 (p368-Cx43) usually migrate at 41 kD (P0 band) [26], while other phosphorylated forms (P1, P2, and rarely P3 bands)

migrate at 42-46 kD range (Fig. 2, Panels A-C). We used the ratio of the P1+P2 bands to the P0 band as a measure of Cx43 "phosphorylation".

Immunohistochemistry (IHC)

IHC was used for Cx43 quantification (Fig. 3). The hearts were fixed in 10% formalin, after which, 8 μm thick sections were blocked for 1 hour at room temperature and were incubated with anti-Cx43 antibodies (Cell Signaling Technology, Danvers, MA, USA) overnight at 4°C. Afterward, sections were stained with anti-rabbit HRP-conjugated antibody (Cell Signaling). Photomicrographs with original magnification ×40 were taken from the apical, mid, and basal left ventricle. Both epicardial and endocardial regions were imaged. Cx43 was quantified with the use of a grid that divided the field of view into 200 squares, and the 200 intersection points in the grid were scored 1 (present) or 0 (absent) for Cx43. The results were expressed as the percentage area occupied by Cx43 to the total area examined (excluding pseudospaces) [27].

Immunolabeled slides were viewed using a Zeiss Axioskop epi-fluorescence light microscope (Carl Zeiss, Inc, Thornwood, NY, USA). Images were imported into ImageJ for processing. In addition, high-magnification double-staining IHC was used to assess Cx43 lateralization (see Supplement).

Functional assessment of Cx43 with a fluorescent dye diffusion technique

Fresh hearts were obtained from *WT*, *ACE 8/8*, and *ACE 8/8* treated mice. A sample from each heart was placed front up in phosphate buffered saline at 37°C, the left ventricle was

punctured with a 27-gauge needle, and the sample was incubated with a droplet of 0.5% Lucifer yellow (LY) and 0.5% Texas Red dextran (TXD) in 150 mM of LiCl solution. After 15 minutes of incubation, the samples were fixed in 4% formaldehyde for 30 minutes, washed in phosphate-buffered saline, frozen in liquid nitrogen, and sliced into 14-micron sections with a Leica 3050S cryostat. The sections were mounted on microscope slides and were examined on a Leica DM5000 B epifluorescence microscope. Digital images of the spread of LY and TXD were obtained. The measurement of the dye spread was performed with ImageJ software. LY is membrane-impermeant, but diffuses through gap junctions, whereas the large-molecular weight TXD does not cross gap junctions and stains only the injected cells. The length of the TXD staining was subtracted from the length of the LY spread at the same site. Dye spread in longitudinal and transverse directions was assessed. The difference in the spreading of LY, which was associated with connexin channels, was determined in the hearts of the control group, the *ACE 8/8* mice, and the *ACE 8/8* treated mice.

Cell isolation and patch clamping

Ventricular cardiac cells were isolated from 5- to 6-wk-old heparinized mice. The explanted hearts were perfused with the perfusion buffer containing 113 mM NaCl, 4.7 mM KCl, 1.2 mM $MgSO_4$, 0.6 mM Na_2HPO_4, 0.6 mM KH_2PO_4, 12 mM $NaHCO_3$, 10 mM $KHCO_3$, 10 mM HEPES, 30 mM taurine, 10 mM BDM (2,3-butanedione monoxime), 0.032 mM Phenol Red, and 0.1% glucose (pH 7.4), at 37°C for 3 min. The hearts were then enzymatically digested using 738 U/ml Worthington type II collagenase dissolved in perfusion buffer for 3 min and 15 sec. After trimming off atria, both

ventricles were minced into small pieces in the stop buffer containing 12.5 μM $CaCl_2$ and 5-10% FBS, and gently triturated with a Pasteur pipette. The cell suspension was passed through 100 μm cell strainer, and the cells were collected by centrifugation at 30xg for 3 min. To remove BDM, the cell pellets were washed 3 times with control solution: 133.5 mM NaCl, 4 mM KCl, 1.2 mM $NaH2PO_4$, 10 mM HEPES, 1.2 mM $MgSO_4$, 0.2% glucose and 0.1% BSA (PH 7.4), with $CaCl_2$ gradually incremented from 200 μM to 1mM in each wash. Finally, the cells were suspended in MEM medium containing 1% insulin-transferrin-selenium (Gibco), 1% glutamine, 0.1% BSA and 1% penicillin-streptomycin for patch clamp experiments.

Sodium current was measured in isolated ventricular myocytes with an Axopatch 200B amplifier (Molecular Devices, Sunnyvale, CA) in whole cell configuration. Data acquisition was performed at a sampling rate of 20 kHz and low-pass filtered at 10 kHz. Data recording and analysis were done with the pClamp8 software suite (Molecular Devices) and OriginPro 8 (Originlab, Northampton, MA). All experiments were carried out at room temperature. Myocytes were plated on glass cover slips and were perfused with a low-sodium Tyrode solution containing 100 mM N-methyl-D-glucamine, 15 mM NaCl, 20 mM tetramethylammonium chloride, 5 mM CsCl , 1 mM $MgCl_2$, 10 mM glucose, 3 mM 4-aminopyridine, 2 mM $MnCl_2$, 10 mM HEPES, and 1 mM $CaCl_2$ 1 (final pH 7.4 with CsOH). Patch electrodes were filled with an electrode solution containing 20 mM CsCl, 20 mM tetraethylammonium chloride, 80 mM glutamic acid, 10 mM NaCl, 1 mM $MgCl_2$, 5 mM MgATP, 0.3 mM Li_2GTP, 10 mM HEPES, 10 mM EGTA, 0.13 mM $CaCl_2$ (corresponding to $[Ca^{2+}]_{free}$ of < 10 nM). Electrode solution pH was adjusted to

7.2 with CsOH. Electrodes used for these experiments had access resistances between 1.0 and 1.5 MΩ.

Statistical analysis

Values are presented as mean ± SD, except for the patch clamp values which are reported as mean ± SE. Student *t*-tests, one-way ANOVA with post hoc tests of significance (Dunnett's multiple comparison or Tukey's honest significance tests), and Fisher's exact tests for 2x2 tables were used where appropriate, and a value of $P<0.05$ was considered statistically significant.

The authors had full access to the data and take responsibility for its integrity. All authors have read and agree to the manuscript as written.

Results

Compared to *WT* mice, ten-week old *ACE 8/8* mice showed low QRS amplitude, indiscernible surface P waves, irregular rhythm because of variable sinus-exit and AV blocks, and shortened ventricular refractory periods (as measured using QT and VERP) (Table 1). The HV interval was significantly prolonged in *ACE 8/8* mice (Fig. 1 and Table 2), consistent with ventricular conduction slowing. Intermittent AV block with short periods of 1:1 conduction intermixed with higher degree block prevented the measurement of AH interval in *ACE 8/8* mice.

In addition, *ACE 8/8* mice had frequent ventricular premature complexes and spontaneous non-sustained VT. EPS induced VT in 7 out of 8 untreated *ACE 8/8* mice compared to only 1 in 23 *WT* mice ($P<0.0001$; Fig 1, Panel E).

In *ACE 8/8* mice, total ventricular Cx43 and the ratio of phosphorylated Cx43 were decreased to less than 15% and 50% of *WT*, respectively (Fig. 2). IHC staining confirmed the reduction in Cx43 (area percentage was reduced to less than 30% of *WT*) and showed the heterogeneous distribution and lateralization of Cx43 in *ACE 8/8* mice (Fig. 3 and Fig. S1). The dye diffusion technique showed significant reduction in diffusion speed in *ACE 8/8* ventricles to less than 70% of the baseline, which predominantly affected the longitudinal conductance (Fig. 4).

Voltage clamp analysis did not show a significant difference in peak sodium current density between *WT* and *ACE 8/8* mice (Fig 5, Panel A). The conductance and steady-

state inactivation curves were slightly shifted to left in *ACE 8/8* cells in comparison to *WT* cells (Fig 5, Panel B). Based on current clamp experiments, the resting membrane potential was -72.1±1.9 mV (*n*=5) in *WT* compared to -71.1±3.4 mV (*n*=5) in *ACE 8/8* mice (P=NS).

The primary effect of treatment with captopril or losartan on *WT* mice was shortening of AV nodal conduction (AV block cycle length and VERP) in the captopril treated and prolongation of AV nodal conduction in the losartan treated mice [28]. There was no significant change in sinus rate, surface PR and QT intervals, atrial and VERP, or VT inducibility.

Nineteen four-week old *ACE 8/8* mice were placed on captopril treatment, and eighteen mice were started on losartan. Four mice in the captopril group and four in the losartan died spontaneously before EPS at ten week of age. Fifteen captopril treated mice (10 male and 5 female) and fourteen losartan treated mice (7 male and 7 female) reached 10 week of age. Therefore, combined survival rate from four to ten weeks was 0.78±0.07, compared to 0.13±0.07 in a group of twenty three untreated mice (P<0.0001). Moreover, intracardiac recordings demonstrated a significant shortening of HV after treatment, but no significant change in VERP (Table 2).

Pharmacological RAS inhibition resulted in increased total Cx43 and an improved Cx43 phosphorylation ratio (Fig. 2, Panels B, C, F, and G). The results achieved statistical significance for total Cx43 in the captopril group and the Cx43 ratio in both groups.

Combining losartan and captopril results, treatment increased total Cx43 2.4-fold (P=0.01) and the phosphorylation ratio 2.3-fold (P=0.005).

IHC staining and dye diffusion results paralleled those expected from Western blotting. IHC showed a significant increase in Cx43 area percentage after treatment with captopril and losartan (Fig. 3). The dye diffusion speed recovered to 97% of the baseline compared to 68% in untreated *ACE 8/8* mice after treatment (Fig. 4).

VT was induced in only 1 out of 8 captopril treated *ACE 8/8* that underwent programmed stimulation and in 2 out of 7 losartan treated mice, compared to 7 out of 8 control untreated *ACE 8/8* mice (P<0.01). There was a strong association between improvement in Cx43 and lack of VT inducibility (Fig. 6, both total Cx43 and the phosphorylation ratio were significantly higher in non-inducible mice). No gender difference in response to treatment was noted.

Discussion

Excessive activity of the RAS system has been associated with sudden death in humans, and inhibition of this system reduces arrhythmic risk [1-4]. Previously, we have shown that a mouse model of cardiac RAS activation suffers from tachycardia-induced sudden death, and the heart has reduced Cx43 amount and phosphorylation [11]. This represented strong circumstantial evidence that Cx43 changes were responsible for the arrhythmic risk in this model of RAS activation. The severity of decrease in Cx43 in *ACE 8/8* mice (≈15% of *WT*) is comparable to other mice models [29] with reduced Cx43 and increased arrhythmic risk and further corroborates the link between Cx43 and arrhythmia. Now, we show that pharmacological inhibition of RAS activity results in significant improvements in sudden death and VT inducibility in this model. This improvement parallels the partial reversal of the decreased total and phosphorylated Cx43 levels as measured by immunoblotting, increased area percentage of end-place Cx43 obtained from IHC staining, and recovery of gap junctional conductance demonstrated by dye diffusion experiments.

As described previously and confirmed in the current study, *ACE 8/8* mice suffer from severe atrial dilatation and eventual atrial standstill with variable and intermittent AV block due to diffuse atrial fibrosis and ventricular conduction abnormality, manifested as HV prolongation. Nevertheless, the primary cause of death in these mice is ventricular tachycardia and not bradycardia [12]. Considering the clinical relevance of ventricular tachycardia in high AngII states, we decided to focus on the ventricular phenotype in this study where fibrosis is minimal.

The finding that both captopril and losartan had largely comparable effects on Cx43 points to the importance of the AT_1 receptor in the modulation of Cx43. If the angiotensin II receptor type-2 (AT_2) receptor or bradykinin breakdown were the primary mediators of the effect, we might have expected to see divergence between the effects of captopril and losartan. Our results are consistent with *in vivo* studies that have demonstrated that ARBs prevent Cx43 dephosphorylation [30,31]. This is in contrast to *in vitro* studies that have found that AT_1 agonists increase total and phosphorylated Cx43 [32,33]. It has been suggested that the discrepancy between *in vitro* and *in vivo* effects of AngII on Cx43 is possibly because AngII increases Cx43 during short exposures and decreases it in chronically elevated states [16].

In this paper, we have focused on Cx43 as the main mediator of the abnormal phenotype in *ACE 8/8* mice. While our results primarily show an association between abnormalities of Cx43 and an abnormal electrophysiological phenotype, the close relationship between an improvement in the phenotype and recovery of Cx43 function and the similarity of the arrhythmic phenotype to other mice models with reduced Cx43 levels strongly suggest a cause and effect relationship [29].

Increased levels of AngII have other electrophysiological effects that may potentially promote VT, but our previous work suggests that other changes are unlikely to play a large role in the *ACE 8/8* arrhythmic phenotype. We did not observe a significant difference in peak sodium current and resting membrane potential between *WT* and *ACE*

8/8 mice. On the other hand, both the conductance and steady-state inactivation curves were shifted to left. These results are consistent with the previous reports on sodium current kinetics in *ACE 8/8* mice [12]. Considering the degree and pattern of alterations, the abnormalities of sodium current kinetics are unlikely to be the main cause of altered ventricular conduction velocity or the pathological phenotype seen in *ACE 8/8* mice. Nevertheless, changes in sodium current with RAS inhibition cannot be excluded as a possible mechanism for the reduction in sudden death seen with treatment in these animals. Another target for AngII regulation is the transient outward potassium current (I_{to}), which in some animal models is inhibited by AngII [7]. It is expected that inhibition of I_{to} should result in prolongation of the VERP. In fact, we observed the opposite in *ACE 8/8* mice. While the exact molecular mechanism of the VERP shortening is not clear, it may promote VT by reducing the reentry wavelength. Nevertheless, VERP did not return to the baseline after treatment with captopril or losartan despite a decrease in VT inducibility and sudden death after treatment, which argues I_{to} does not have a central role in VT inducibility in *ACE 8/8* mice. Moreover, we did not find major alterations in other channels or ventricular fibrosis (in contrast to significant atrial fibrosis) [11]. The observed effect on reducing arrhythmic risk from partial improvement in Cx43 is consistent with the concept of a "safety margin" [34], where the amount of Cx43 available in normal state is many fold more than what is needed to maintain action potential conduction, and conduction velocity is more dependent on Cx43 levels when they are significantly reduced.

Similar to the human situation, we observed heterogeneity in response to pharmacological treatment. Not all mice responded to the same degree, but those *ACE 8/8* mice that were rendered non-inducible after treatment had higher total and phosphorylated Cx43. Possibilities for a lack of a uniform response include intrinsic difference among mice or differences in drug delivery and metabolism.

In summary, pharmacological inhibition of excessive RAS activity resulted in partial reversal of abnormal Cx43 remodeling by increasing the amount and functional recovery of Cx43. This was correlated with a significant reduction in VT inducibility and sudden death.

References

1. Swedberg K, Kjekshus, J (1988) Effects of enalapril on mortality in severe congestive heart failure: results of the Cooperative North Scandinavian Enalapril Survival Study (CONSENSUS). Am. J. Cardiol. 62: 60A-66A.
2. Yusuf S, Sleight, P, Pogue, J, Bosch, J, Davies, R, Dagenais, G (2000) Effects of an angiotensin-converting-enzyme inhibitor, ramipril, on cardiovascular events in high-risk patients. The Heart Outcomes Prevention Evaluation Study Investigators. N. Engl. J. Med. 342: 145-153.
3. Pitt B, Zannad, F, Remme, WJ, Cody, R, Castaigne, A, Perez, A, Palensky, J, Wittes, J (1999) The effect of spironolactone on morbidity and mortality in patients with severe heart failure. Randomized Aldactone Evaluation Study Investigators. N. Engl. J. Med. 341: 709-717.
4. Pitt B, Remme, W, Zannad, F, Neaton, J, Martinez, F, Roniker, B, Bittman, R, Hurley, S, Kleiman, J, Gatlin, M (2003) Eplerenone, a selective aldosterone blocker, in patients with left ventricular dysfunction after myocardial infarction. N. Engl. J. Med. 348: 1309-1321.
5. Crabos M, Roth, M, Hahn, AW, Erne, P (1994) Characterization of angiotensin II receptors in cultured adult rat cardiac fibroblasts. Coupling to signaling systems and gene expression. J. Clin. Invest 93: 2372-2378.
6. Kaibara M, Mitarai, S, Yano, K, Kameyama, M (1994) Involvement of Na^{+}-H^{+} antiporter in regulation of L-type Ca^{2+} channel current by angiotensin II in rabbit ventricular myocytes. Circ. Res. 75: 1121-1125.

7. Caballero R, Gomez, R, Moreno, I, Nunez, L, Gonzalez, T, Arias, C, Guizy, M, Valenzuela, C, Tamargo, J, Delpon, E (2004) Interaction of angiotensin II with the angiotensin type 2 receptor inhibits the cardiac transient outward potassium current. Cardiovasc. Res. 62: 86-95.
8. Ju H, Scammel-La Fleur, T, Dixon, IM (1996) Altered mRNA abundance of calcium transport genes in cardiac myocytes induced by angiotensin II. J. Mol. Cell Cardiol. 28: 1119-1128.
9. Tokuhisa T, Yano, M, Obayashi, M, Noma, T, Mochizuki, M, Oda, T, Okuda, S, Doi, M, Liu, J, Ikeda, Y et al (2006) AT1 receptor antagonist restores cardiac ryanodine receptor function, rendering isoproterenol-induced failing heart less susceptible to Ca2+ -leak induced by oxidative stress. Circ. J. 70: 777-786.
10. Flesch M, Schiffer, F, Zolk, O, Pinto, Y, Stasch, JP, Knorr, A, Ettelbruck, S, Bohm, M (1997) Angiotensin receptor antagonism and angiotensin converting enzyme inhibition improve diastolic dysfunction and Ca(2+)-ATPase expression in the sarcoplasmic reticulum in hypertensive cardiomyopathy. J. Hypertens. 15: 1001-1009.
11. Xiao HD, Fuchs, S, Campbell, DJ, Lewis, W, Dudley, SC, Jr., Kasi, VS, Hoit, BD, Keshelava, G, Zhao, H, Capecchi, MR et al (2004) Mice with cardiac-restricted angiotensin-converting enzyme (ACE) have atrial enlargement, cardiac arrhythmia, and sudden death. Am. J. Pathol. 165: 1019-1032.
12. Kasi VS, Xiao, HD, Shang, LL, Iravanian, S, Langberg, J, Witham, EA, Jiao, Z, Gallego, CJ, Bernstein, KE, Dudley, SC (2007) Cardiac Restricted

Angiotensin Converting Enzyme Overexpression Causes Conduction Defects and Connexin Dysregulation. Am. J. Physiol Heart Circ. Physiol 293: H182-H192.

13. van Veen AA, van Rijen, HV, Opthof, T (2001) Cardiac gap junction channels: modulation of expression and channel properties. Cardiovasc. Res. 51: 217-229.
14. Shaw RM, Rudy, Y (1997) Ionic mechanisms of propagation in cardiac tissue. Roles of the sodium and L-type calcium currents during reduced excitability and decreased gap junction coupling. Circ. Res. 81: 727-741.
15. Kaprielian RR, Gunning, M, Dupont, E, Sheppard, MN, Rothery, SM, Underwood, R, Pennell, DJ, Fox, K, Pepper, J, Poole-Wilson, PA et al (1998) Downregulation of immunodetectable connexin43 and decreased gap junction size in the pathogenesis of chronic hibernation in the human left ventricle. Circulation 97: 651-660.
16. Teunissen BE, Jongsma, HJ, Bierhuizen, MF (2004) Regulation of myocardial connexins during hypertrophic remodelling. Eur. Heart J 25: 1979-1989.
17. Yao JA, Hussain, W, Patel, P, Peters, NS, Boyden, PA, Wit, AL (2003) Remodeling of gap junctional channel function in epicardial border zone of healing canine infarcts. Circ. Res. 92: 437-443.
18. Efimov IR (2006) Connections, connections, connexins: towards systems biology paradigm of cardiac arrhythmia. J. Mol. Cell Cardiol. 41: 949-951.
19. Vinet A, Roberge, FA (1994) The dynamics of sustained reentry in a ring model of cardiac tissue. Ann. Biomed. Eng 22: 568-591.

20. Lampe PD, TenBroek, EM, Burt, JM, Kurata, WE, Johnson, RG, Lau, AF (2000) Phosphorylation of connexin43 on serine368 by protein kinase C regulates gap junctional communication. J. Cell Biol. 149: 1503-1512.

21. Laird DW, Revel, JP (1990) Biochemical and immunochemical analysis of the arrangement of connexin43 in rat heart gap junction membranes. J. Cell Sci. 97 (Pt 1): 109-117.

22. Ek-Vitorin JF, King, TJ, Heyman, NS, Lampe, PD, Burt, JM (2006) Selectivity of connexin 43 channels is regulated through protein kinase C-dependent phosphorylation. Circ. Res. 98: 1498-1505.

23. Solan JL, Lampe, PD (2007) Key connexin 43 phosphorylation events regulate the gap junction life cycle. J. Membr. Biol. 217: 35-41.

24. van Kats JP, Danser, AH, van Meegen, JR, Sassen, LM, Verdouw, PD, Schalekamp, MA (1998) Angiotensin production by the heart: a quantitative study in pigs with the use of radiolabeled angiotensin infusions. Circulation 98: 73-81.

25. Donoghue M, Wakimoto, H, Maguire, CT, Acton, S, Hales, P, Stagliano, N, Fairchild-Huntress, V, Xu, J, Lorenz, JN, Kadambi, V et al (2003) Heart block, ventricular tachycardia, and sudden death in ACE2 transgenic mice with downregulated connexins. J Mol Cell Cardiol. 35: 1043-1053.

26. Solan JL, Fry, MD, TenBroek, EM, Lampe, PD (2003) Connexin43 phosphorylation at S368 is acute during S and G2/M and in response to protein kinase C activation. J. Cell Sci. 116: 2203-2211.

27. Morita N, Sovari, AA, Xie, Y, Fishbein, MC, Mandel, WJ, Garfinkel, A, Lin, SF, Chen, PS, Xie, LH, Chen, F et al (2009) Increased susceptibility of aged hearts to ventricular fibrillation during oxidative stress. Am. J. Physiol Heart Circ. Physiol 297: H1594-H1605.

28. Iravanian S, Sovari, AA, Dudley, SC (2010) Renin-Angiotensin System Modulation of Atrioventricular Nodal Conduction. Heart Rhythm 7: S170.

29. Gutstein DE, Morley, GE, Tamaddon, H, Vaidya, D, Schneider, MD, Chen, J, Chien, KR, Stuhlmann, H, Fishman, GI (2001) Conduction slowing and sudden arrhythmic death in mice with cardiac-restricted inactivation of connexin43. Circ Res 88: 333-339.

30. Fischer R, Dechend, R, Gapelyuk, A, Shagdarsuren, E, Gruner, K, Gruner, A, Gratze, P, Qadri, F, Wellner, M, Fiebeler, A et al (2007) Angiotensin II-induced sudden arrhythmic death and electrical remodeling. Am. J. Physiol Heart Circ. Physiol 293: H1242-H1253.

31. De Mello WC, Specht, P (2006) Chronic blockade of angiotensin II AT1-receptors increased cell-to-cell communication, reduced fibrosis and improved impulse propagation in the failing heart. J. Renin. Angiotensin. Aldosterone. Syst. 7: 201-205.

32. Polontchouk L, Ebelt, B, Jackels, M, Dhein, S (2002) Chronic effects of endothelin 1 and angiotensin II on gap junctions and intercellular communication in cardiac cells. FASEB J 16: 87-89.

33. Inoue N, Ohkusa, T, Nao, T, Lee, JK, Matsumoto, T, Hisamatsu, Y, Satoh, T, Yano, M, Yasui, K, Kodama, I et al (2004) Rapid electrical stimulation of

contraction modulates gap junction protein in neonatal rat cultured cardiomyocytes: involvement of mitogen-activated protein kinases and effects of angiotensin II-receptor antagonist. J. Am. Coll. Cardiol. 44: 914-922.

34. Kleber AG, Rudy, Y (2004) Basic mechanisms of cardiac impulse propagation and associated arrhythmias. Physiol Rev. 84: 431-488.

Funding

This work was supported by National Institute of Health grants R01 HL085558 (SCD, KEB), R01 HL073753 (SCD), P01 HL058000 (SCD), DK039777 (KEB), American Heart Association (AHA) national scientist development grant (HDX), and AHA postdoctoral fellowship (SI).

Conflict of Interest

The authors have no conflict of interest to disclose.

Table Legends

1. Table showing various surface ECG and invasive EPS parameters in *WT* compared to untreated and pharmacologically treated *ACE 8/8* mice. All the numbers are in ms, except for R wave, which is in mV. *RR*: cycle length, *PR*: PR interval, *QRSd*: QRS duration, *QT*: QT interval, *R wave*: QRS vector amplitude, There was significant difference in QRS amplitude and QT interval between *WT* and *ACE 8/8* mice.
2. Table showing intracardiac His recordings in *WT* compared to untreated and pharmacologically treated *ACE 8/8* mice. *AH*: interval between atrial activity and His bundle recording. *HV*: interval from His bundle recording to the beginning of ventricular activity. There is a significant increase in HV interval in *ACE 8/8* mice, which is reduced after treatment with either captopril or losartan.

Figure Legends

1. **(A)-(D)** Surface and intracardiac electrograms from *WT* **(A)**, untreated *ACE 8/8* **(B)**, captopril treated *ACE 8/8* **(C)**, and losartan treated *ACE 8/8* **(D)** mice. Note the prolonged AH and HV intervals in *ACE 8/8* mouse, reversed after treatment with either captopril or losartan. The surface ECG are to the same scale, however intracardiac signals are depicted with different vertical scales. **(E)** An example of induced VT during programmed ventricular stimulation in untreated *ACE 8/8* mice.
2. **(A)** An immunoblot comparing Cx43 in *WT* and *ACE 8/8* mice. The top row shows total Cx43. P0 runs at 41 kDa, whereas, P1 and P2 are mostly phosphorylated and migrate at 44-46 kDa. Note the reduction in total and phosphorylated Cx43 in *ACE 8/8*. GAPDH staining was used for loading control. **(B)** Immunoblot showing the effect of captopril treatment on Cx43 in *ACE 8/8* mice. **(C)** Immunoblot showing the effect of losartan treatment on Cx43. **(D)** Normalized total Cx43 in *WT* vs. *ACE 8/8* mice ventricles. **(E)** (P1+P2)/P0 ratio in *WT* vs. *ACE 8/8* mice. **(F)** Normalized total Cx43 in *ACE 8/8* mice after treatment with captopril and losartan (*n*=12 for untreated, *n*=10 for captopril and n=8 for losartan treated groups). **(G)** (P1+P2)/P0 ratio in *ACE 8/8* mice after treatment with captopril and losartan (*n*=13 for untreated, *n*=10 for captopril and *n*=11 for losartan treated groups). Student *t*-test was used to analyze **(C)** and **(D)**, one-way ANOVA was used for **(E)** and **(F)**, with Dunnett's test of significance to compare each treatment group with the control (* $P<0.01$, ** $P<0.05$). Error bars represent mean ± SEM.

3. IHC stained images showing representative fields from left ventricular myocardium of *WT* **(A)**, *ACE 8/8* **(B)**, captopril treated *ACE 8/8* **(C)**, and losartan treated *ACE 8/8* **(D)** mice. Cx43 is stained brown. **(E)** Cx43 area percentage (see text) is significantly reduced in *ACE 8/8* ventricle compare to *WT* and recovered after treatment (combined captopril and losartan group).
4. Results of merged fluorescent dye transfer images in *WT* **(A)**, *ACE 8/8* **(B)**, and treated *ACE 8/8* **(C)** mice. Red represents TXD staining that is confined to the injected cell, whereas green depicts LY staining that diffuses through gap junctions. Gap junctional conductance correlates with TXD-corrected LY spread. There is a significant reduction in dye spread in *ACE 8/8* mice, which partially recovers after treatment **(D)**. This effect is more pronounced in the longitudinal direction **(E)** (*n*=7 for WT, *n*=7 for ACE 8/8 no treatment group, and *n*=7 for the combined treatment group).
5. **(A)** Current-voltage plot for sodium current in *WT* and *ACE 8/8* mice. The experiments were performed with 10 ms pulses over a voltage range of -90 to +55 mV. The peak current density was -38.6±2.5 pA/pF (*n*=7) in *WT* compared to -42.7±12.6 pA/pF (*n*=3) in *ACE 8/8* (P=NS). (B) Comparison of sodium current conductance (right) and steady-state inactivation (left) in *WT* and *ACE 8/8* mice. The conductance was calculated based on the protocol presented in (A), whereas for the steady-state inactivation, holding potentials ranging from -120 to -20 mV were sustained for 1 s and followed by a 10 ms test pulse of -10 mV. The membrane voltage at half-maximal conductance was -34.2±1.5 mV (*n*=7) and -42.6±2.9 mV (*n*=3) in *WT* and *ACE 8/8*, respectively (P=0.02). The membrane

voltage at 50% inactivation was -70.8±2.1 mV (*n*=4) and -76.0±4.0 (*n*=4), respectively (P=NS).

6. **(A)** A representative immunoblot showing the association between VT inducibility and Cx43 expression in *ACE 8/8* mice. GAPDH was used as a loading control. **(B)** Total Cx43 as a function of VT inducibility (*n*=6 for non-inducible and *n*=8 for inducible groups). **(C)** (P1+P2)/P0 as a function of VT inducibility (*n*=7 for non-inducible and *n*=9 for inducible groups). Error bars represent mean ± SEM.

Table 1

		ACE 8/8			
	WT **(n=11)**	**Untreated (n=20)**	**Captopril treated (n=12)**	**Losartan treated (n=14)**	**Combined Treated (n=26)**
PR	43±4				
QRSd	19.6±1.3	20.1±2.1	18.8±1.5	19.3±1.2	19.1±1.3
QT	53±5	44±8*	46±4	48±8	47±6
VERP	54±7	44±13*	50±12	43±9	47±11
R wave	0.35±0.08	0.05±0.02*	0.10±0.06**	0.12±0.09**	0.11±0.08**

* P<0.05 vs. WT
** P<0.05 vs. untreated

Table 2

		ACE 8/8			
	WT **(n=8)**	**Untreated (n=5)**	**Captopril treated (n=4)**	**Losartan treated (n=4)**	**Combined Treated (n=8)**
AH (ms)	28±5	N/A	30±6	30±12	30±10
HV (ms)	10±1	29±4*	13±2**	13±6**	13±4**

* P<0.05 vs. WT
** P<0.05 vs. untreated

Figure 1

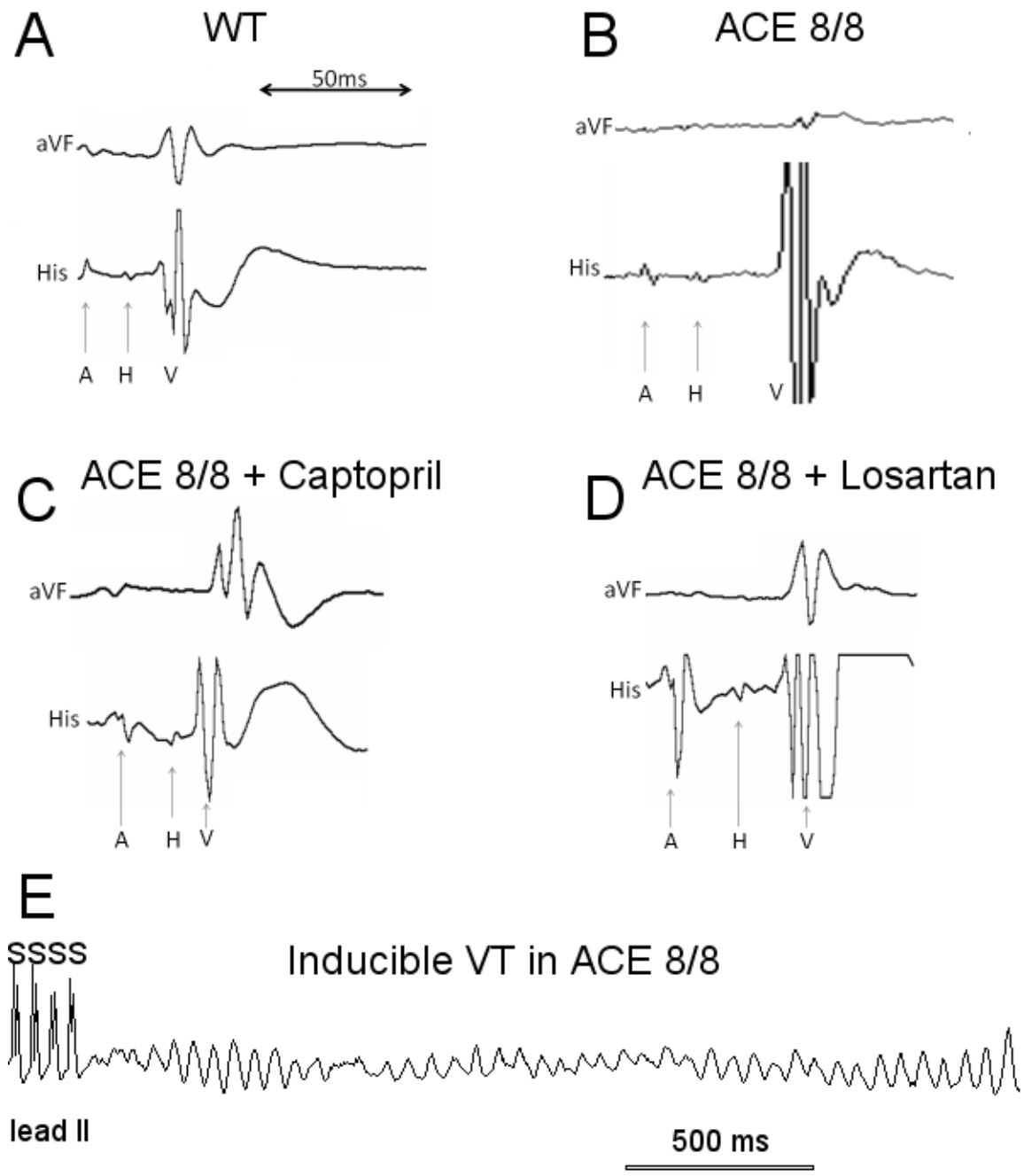
A
WT
50ms
aVF
His
A H V
B
ACE 8/8
aVF
His
A H V
C
ACE 8/8 + Captopril
aVF
His
A H V
D
ACE 8/8 + Losartan
aVF
His
A H V
E
SSSS
Inducible VT in ACE 8/8
lead II
500 ms

Figure 2

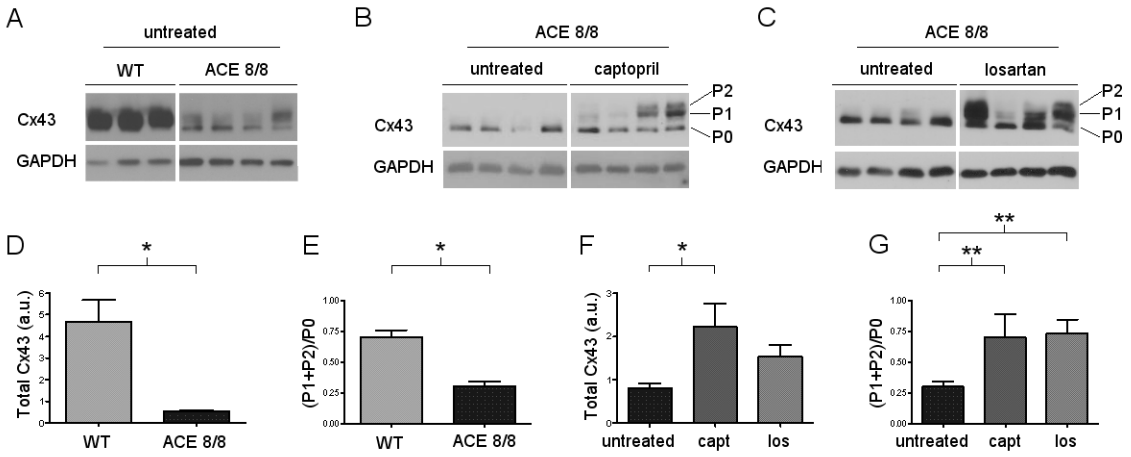
A
untreated
WT
ACE 8/8
Cx43
GAPDH
B
ACE 8/8
untreated
captopril
Cx43
GAPDH
P2
P1
P0
C
ACE 8/8
untreated
losartan
Cx43
GAPDH
P2
P1
P0
D
*
Total Cx43 (a.u.)
WT
ACE 8/8
E
*
(P1+P2)/P0
WT
ACE 8/8
F
*
Total Cx43 (a.u.)
untreated
capt
los
G
**
**
(P1+P2)/P0
untreated
capt
los

Figure 3

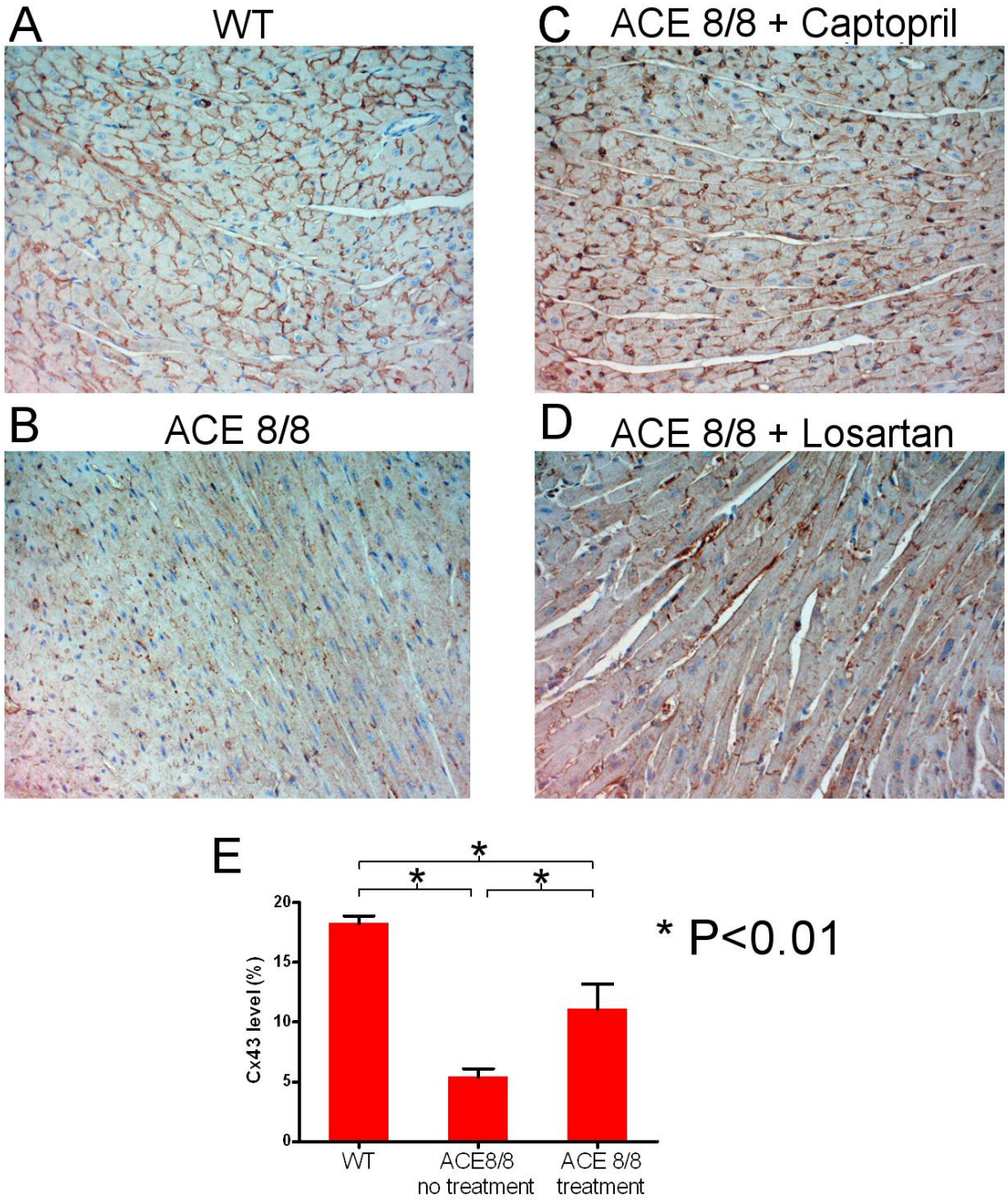
A
WT
C
ACE 8/8 + Captopril
B
ACE 8/8
D
ACE 8/8 + Losartan
E
*
*
*
Cx43 level (%)
20
15
10
5
0
WT
ACE8/8
no treatment
ACE 8/8
treatment
* P<0.01

Figure 4

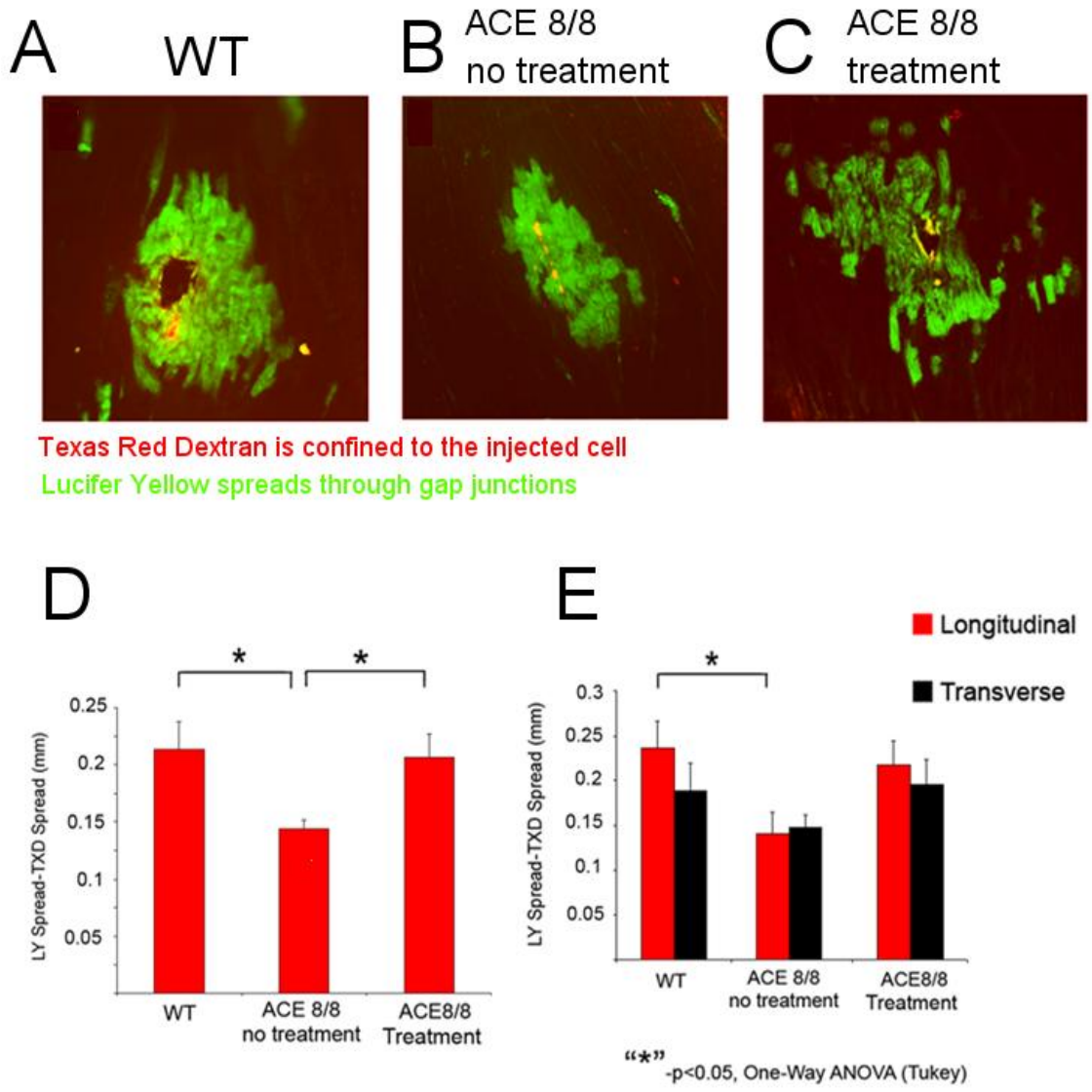
A WT
B ACE 8/8 no treatment
C ACE 8/8 treatment
Texas Red Dextran is confined to the injected cell
Lucifer Yellow spreads through gap junctions
D
LY Spread-TXD Spread (mm)
0.25
0.2
0.15
0.1
0.05
*
*
WT
ACE 8/8 no treatment
ACE8/8 Treatment
E
Longitudinal
Transverse
LY Spread-TXD Spread (mm)
0.3
0.25
0.2
0.15
0.1
0.05
*
WT
ACE 8/8 no treatment
ACE8/8 Treatment
"*" -p<0.05, One-Way ANOVA (Tukey)

Figure 5

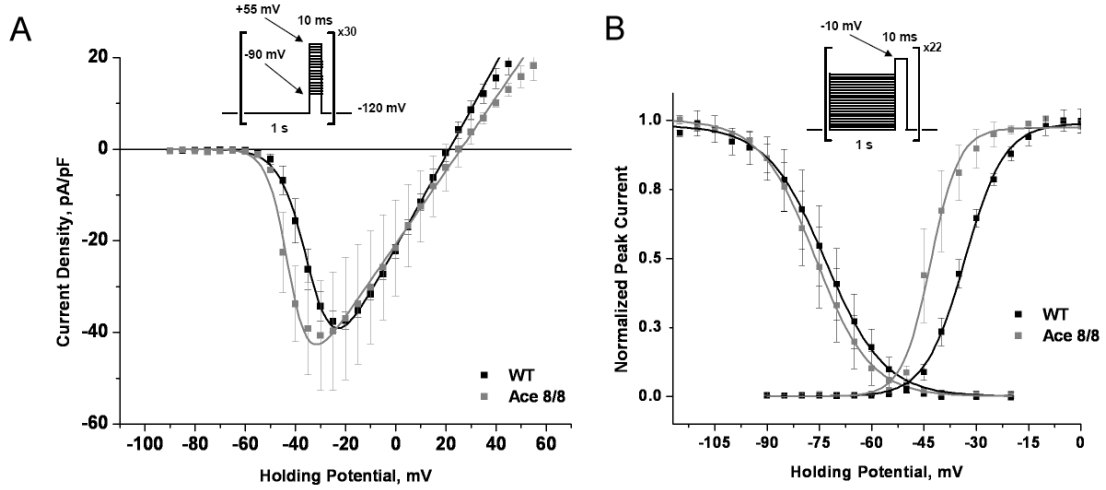
A
+55 mV
10 ms
x30
-90 mV
-120 mV
1 s
Current Density, pA/pF
Holding Potential, mV
WT
Ace 8/8
B
-10 mV
10 ms
x22
1 s
Normalized Peak Current
Holding Potential, mV
WT
Ace 8/8

Figure 6

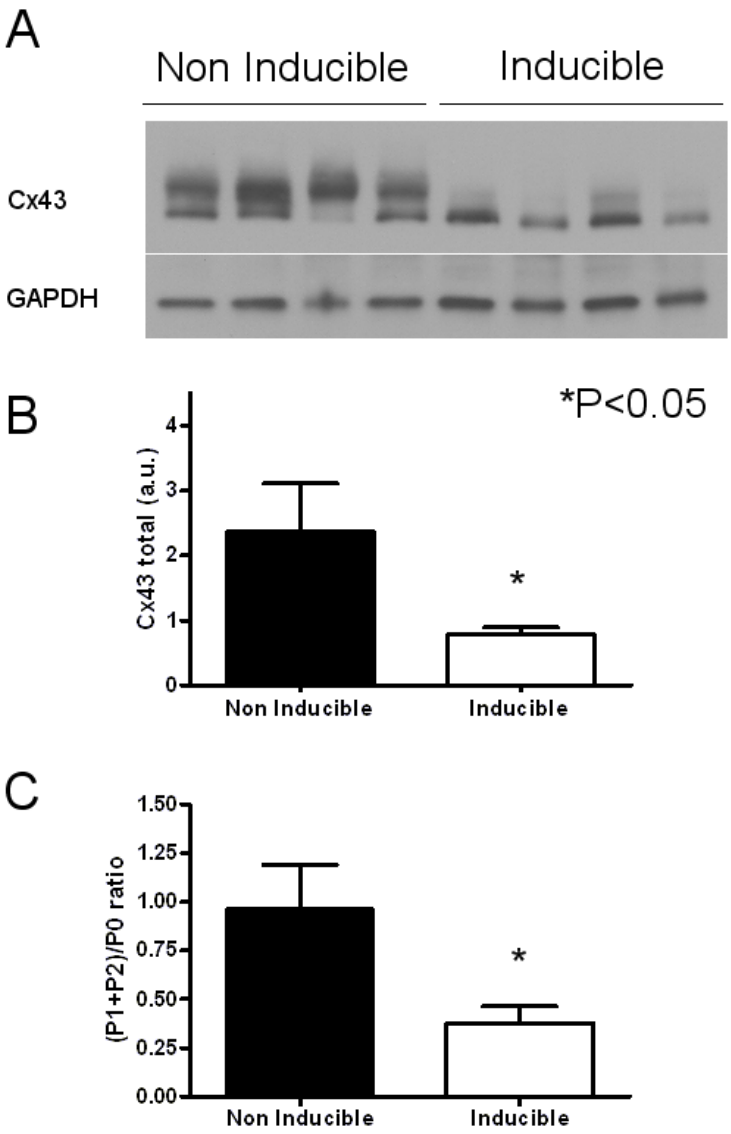
A
Non Inducible
Inducible
Cx43
GAPDH
B
*P<0.05
Cx43 total (a.u.)
0
1
2
3
4
*
Non Inducible
Inducible
C
(P1+P2)/P0 ratio
0.00
0.25
0.50
0.75
1.00
1.25
1.50
*
Non Inducible
Inducible